PAPER

Microwave-assisted synthesis and *in vitro* osteogenic analysis of novel bioactive glass fibers for biomedical and dental applications

IOP ebooks™

Bringing you innovative digital publishing with leading voices to create your essential collection of books in STEM research.

Start exploring the collection - download the first chapter of every title for free.

Biomedical Materials

PAPER

Microwave-assisted synthesis and *in vitro* osteogenic analysis of novel bioactive glass fibers for biomedical and dental applications

Hina Khalid[1], **Fatima Suhaib**[2], **Shahreen Zahid**[2], **Suhaib Ahmed**[3], **Arshad Jamal**[4], **Muhammad Kaleem**[2] and **Abdul Samad Khan**[5,6]

1   Interdisciplinary Research Centre in Biomedical Materials, COMSATS University Islamabad, Lahore Campus, Lahore 54000, Pakistan
2   Department of Dental Materials, Army Medical College, National University of Medical Sciences, Rawalpindi 44000, Pakistan
3   Department of Pathology, Riphah International University, Islamabad 44000, Pakistan
4   Faculty of Allied and Health Sciences, Imperial College of Business Studies, Lahore 54000, Pakistan
5   Department of Restorative Dental Sciences, College of Dentistry, Imam Abdulrahman Bin Faisal University, Dammam 31441, Saudi Arabia
6   Author to whom any correspondence should be addressed.

E-mail: akhan@iau.edu.sa

Abstract

Glass fiber-based materials have gained interest for use in biomedical and dental applications. The aim of this study was to make E-glass fiber bioactive by a novel method using the microwave irradiation technique. Industrial E-glass fibers were used after surface activation with the hydrolysis method. The ratio of calcium and phosphorous precursors was set at 1.67. After maintaining the pH of the calcium solution, E-glass fibers in two ratios, i.e. 30% (nHA/E30) and 50% (nHA/E50) wt/wt, were added. The phosphorous precursor was added later and the solution was irradiated in a microwave to obtain nano-hydroxyapatite (nHA) particles on E-glass fibers. The structural, physical and *in vitro* biocompatibility analyses of the resulting materials were conducted. The expression of osteopontin (OPN) and collagen (Col) type 1 was measured by reverse transcription polymerase chain reaction (RT-PCR) and comparison was made between all the groups. Fourier transform infrared spectroscopy and x-ray diffraction showed characteristic peaks of nHA, and a change in the peak intensities was observed with an increase in the concentration of E-glass fibers. Scanning electron microscopic (SEM) images confirmed the homogenous adhesion of nHA spherical particles all over the fibers. Cell viability with mesenchymal stem cells showed growth, proliferation, and adhesion. All the materials were able to upregulate the expression of the OPN and Col, where gene expression was highest in nHA followed by nHA/E30 and nHA/E50. The bioactive glass fibers were synthesized in the shortest time and showed osteogenic properties. These materials have the potential for use in bone tissue engineering, dental prosthesis, and tooth restoration.

1. Introduction

It is desirable for dental and biomedical materials to possess bioactive properties and they must demonstrate biocompatibility with hard and soft tissues. Glass fiber-based biomedical materials have gained interest for clinical application due to their superior mechanical and physical properties [1] and their ability to remain inert in a biological environment [2]. They are an amorphous, non-heterogeneous 3D mesh of haphazardly arranged SiO_2 (54.5% wt), Al_2O_3 (14.5% wt), CaO (17% wt), MgO (4.5% wt), B_2O_3

(8.5% wt), and Na_2O (0.5% wt) [3, 4]. They are durable and non-resorbable and there are many types; however, E-glass fibers and S-glass fibers have been mainly used for clinical applications [5, 6]. Adding E-glass fiber to the polymer significantly improves the material's mechanical properties [7] and was recently proposed as bone anchored material implant material in dental, orthopedic, and craniofacial surgeries [8, 9]. They showed potential for use as an implant when combined with bioactive glass (BAG) [10]. However, BAG was embedded in resin matrix as loose particles and had no linkage with glass fibers. It was suggested

that the additional coating of bioactive materials on the fiber-reinforced composite structure might have helped to control the initial ion release rate and thus aid osseointegration [11].

Among bioactive materials, hydroxyapatite (HA) is considered to be one of the most biocompatible and bioactive materials and has gained wide acceptance in medicine and dentistry in recent years [12, 13]. With the advent of new technologies, several methods have been developed to prepare synthetic HA, including wet precipitation [14], chemical precipitation [15], the sol–gel method [16], and microwave irradiation [17]. In all these methods, the structure, phase purity, porosity, surface properties and sintering temperature are important factors affecting HA and its properties for the adhesion of cells and proliferation [18]. The osteoconductivity of the material depends on the cellular behavior on the surface of a biomaterial and it is now a well-known fact that surface chemistry and topography govern the biological response to a biomedical material [19].

The microwave-assisted synthesis approach has been recently used for the preparation of composites, polymers, and ceramics [20]. Our group synthesized an nHA and nHA/carbon nanotube by microwave-assisted wet precipitation [21]. The technique furnishes the product with high purity in a much shorter time. In this study, the idea was conceived that the *in situ* synthesis of nHA would be linked on an E-glass fiber surface to make them bioactive with potential biomedical and dental applications.

2. Methodology

2.1. Preparation of E-glass
To synthesize the nHA/E-glass fibrous material, the obtained industrial E-glass fibers were initially cut into small pieces by using a fine surgical blade (no. 12) and they were heat treated at 250 °C in a drying furnace (WiseVen, South Korea) with a heating ramp of 10 °C min^{-1} to remove any surface impurities. Then, the E-glass fibers were refluxed with 10% HCl (Sigma Aldrich, USA) for 3 h and then acid activated fibers were washed with distilled water to remove all acidic contents followed by drying at 110 °C for 2 h. The surface activated E-glass fibers were stored in a desiccator.

2.2. Synthesis of nHA/E-glass fibers
Analytical grade calcium nitrate (Ca(NO$_3$)$_2$.4H$_2$O) (Sigma Aldrich, USA) and diammonium hydrogen phosphate ((NH$_4$)$_2$HPO$_4$) (AppliChem, Germany) were used as precursors for the synthesis of nHA and nHA/E-glass. nHA was synthesized as described previously by our group [22]. The Ca/P ratio was set at 1.67 to prepare stoichiometric nHA as a control. To synthesize the nHA/E-glass fibers, 1.0 M Ca(NO$_3$)$_2$.4H$_2$O solution was

prepared in deionized water. The pH was maintained at 10 by the dropwise addition of ammonium hydroxide ((NH$_4$)$_2$HPO$_4$; BDH, UK). Then, surface-activated E-glass fibers were added to this solution in increments. The concentration of E-glass was 30% and 50% wt/wt. The Ca(NO$_3$)$_2$.4H$_2$O solution with E-glass fibers was stirred for 30 min at ambient temperature (23 °C ± 2 °C). Then, 0.6 M (NH$_4$)$_2$HPO$_4$ solution was prepared in deionized water and the pH was maintained at 10 by adding (NH$_4$)$_2$HPO$_4$ and this solution was added dropwise to Ca(NO$_3$)$_2$.4H$_2$O solution at a dropping rate of 2 ml min^{-1}. The reaction mixture was then stirred for 30 min (the pH was maintained at 10) before refluxing in a domestic microwave oven (Samsung MW101P) at 1000 W for 3 min (15 s ON:OFF). After microwave irradiation, the reaction mixture was filtered, washed with distilled water and aged in a drying oven at 80 °C for 24 h. The resulting materials with 30% wt and 50% wt E-glass fibers were denoted as nHA/E30 and nHA/E50 respectively, whereas nHA without E-glass fibers was symbolized as nHA/E0. All resulting materials were heat treated at 450 °C for 1 h (ramp rate ≈ 10 °C min^{-1}) and cooled down to room temperature (ramp rate ≈ 10 °C min^{-1}). The resulting products were isolated and characterized for structural, thermal, morphological and *in vitro* biological analysis. To confirm the synthesis of HA, a sub-group of an nHA/E0 sample was heat treated at 1000 °C (ramp rate ≈ 10 °C min^{-1}) for 1 h and the sample was denoted as nHA-ht.

2.3. Characterizations
2.3.1. Fourier transform infrared spectroscopy
Fourier transform infrared spectroscopy (FTIR) was conducted to determine the structural structure of the experimental samples. A photoacoustic cell was used as an accessory with FTIR (Thermo Nicolet 6700, Thermo Fischer Scientific, USA) with the resolution set at 8 cm^{-1}. The spectral range was 4000–400 cm^{-1} and the scan numbers were 256. OMINIC software was used to analyze the spectra.

2.3.2. X-ray diffraction
X-ray diffraction (XRD) was used to evaluate the phase purity and the analysis was carried out on a diffractometer system PERT-PRO using Goniometer geometry (PW3050/60) at room temperature with Cu K-α radiation. The XRD pattern was recorded continuously with 2θ from 20°–80° with a step size of 0.02°.

2.3.3. Thermogravimetric analysis
Thermogravimetric analysis (TGA) was performed on QEX-600 (TA Instruments, UK) using a platinum pan as reference material. The analysis was carried out between 25 °C–500 °C at a rate of 10 °C min^{-1} under an inert nitrogen environment.

2.3.4. Scanning electron microscope

The morphology of the prepared materials and the presence of nHA particles on the E-glass fiber surface were investigated by scanning electron microscope (SEM, Tescan Vega-3 LMU, Czech Republic) at a voltage of 20 KV. Samples were coated (thickness $\approx$ 250A°) in a gold sputter coater (QUORUM) and were evaluated at multiple magnifications.

2.4. Cell viability test

The nHA/E0, nHA/E30 and nHA/E50 sample pellets (6×2 mm^2) were prepared under a compressive pressure of 60 MPa by using a universal testing machine (Testometrics, UK). The pellets were heat treated at 450 °C at a heating ramp of 10 °C min^{-1} and then initially sterilized under UV light for 6 h, then with 70/30 ethanol solution for 30 min, and later irradiated with γ-radiations.

2.4.1. In vitro culture of rat mesenchymal stem cells

After taking institutional ethical permission, rat mesenchymal stem cells were isolated from the femur of 4–5 week-old rats using the direct adherence method. The femur was isolated under sterile conditions. A disposable aseptic syringe was used to draw antibiotic supplemented L-DMEM medium repeatedly in and out of the bone marrow cavity and the cell fractions were collected in a sterile petri dish. The obtained cell suspension was centrifuged at 250 X g for 5 min. The cell pellet was resuspended in L-DMEM (GIbco) containing 10% fetal bovine serum (FBS, Gibco), 0.1% penicillin and streptomycin (GIbco) and transferred to a T25 tissue culture flask. The flasks were incubated at 37 °C in a 5% CO$_2$ incubator. Cells isolated from one rat were cultured in one flask. The first medium was changed after four days. Later on, the medium was changed on alternative days until the cells became 70%–80% confluent. MSC were subcultured at 70%–80% confluence. The cells were trypsinized, counted (dead cells excluded by trypan blue assay) and passaged in T-75 flasks. Second- or third-passage MSC were used for cytotoxicity and SEM analysis.

2.4.2. Cytotoxicity assay

Cellular toxicity was determined by 3-(4,5-Dimethylthiazol-2-yl)-2,5-diphenyltetrasodium bromide (MTT) assay. Immediately, before cell seeding, the pellets were pre-soaked in cell culture medium for an hour. MSC were seeded in a 24-well cell culture plate with $5 * 10^4$ cells per well with or without sample pellets. Cells seeded in wells without sample pellets were used as a positive control (TCP). Post day 3 and 7, the medium was discarded and cells/scaffolds were washed with 1 ml phosphate buffer solution (PBS). Then, 1 ml (0.5 mg ml^{-1}) MTT solution was added to each well and the plate was incubated at 37 °C for 3 h. The MTT solution was discarded and the cells/scaffolds were washed once with 1 ml PBS. To solubilize the formazan crystals, 0.5 ml dimethyl sulfoxide was added to each well and the plate was kept under shaking for 15–20 min. The optical density of the dissolved crystals was measured by using a microplate reader (PR 4100, Bio Rad, USA) at 590 nm. The assay was set up in triplicate with MSC derived from three different rats for each sample. The % viability is represented as mean $\pm$ SD of three independent experiments.

2.5. In vitro osteogenesis analysis

For the osteogenesis analysis, MC3T3-E1 murine osteoblasts (RIKEN Bio Resource Centre, Tsukuba, Ibaraki, Japan) were used. This cell line was maintained in α-minimum essential medium (α-MEM) (GIBCO®) supplemented with 10% FBS (GIBCO®) and 2 mM glutamine under standard conditions at 37 °C and 5% CO$_2$. The medium was changed every third day and the cells were trypsinized with 0.25% trypsin (TryPLE Selec^{TM}, GIBCO®) after 80% confluence. The pellets were immersed in medium overnight and seeded with MC3T3 E-1 cells, maintaining a concentration of 3×10^4/well in 1 ml of α-MEM medium with 10% FBS. The control (tissue culture plate) was also treated in a similar manner. The well plates were stored at 37 °C with 5% CO$_2$ and cells were allowed to grow on the pellets for five days, after which the pellets were removed for RNA extraction. The control samples (cells without pellets) were also removed for RNA extraction.

2.5.1. RNA extraction

On the fifth day of the experiment, total RNA extraction was conducted with an RNA extraction kit (SaMag, Italy) and automated RNA extraction equipment (SaMag, Italy). Each pellet was added to a separate tube. A volume of 220 μl cell lysis buffer was added to the tubes containing the samples and the contents of the tubes were mixed by gentle vortex. The tubes were placed in the automated RNA extraction machine. This method employs anti-RNA coated magnetic beads for RNA extraction. In a reagent cartridge, the lysed cell suspension was sequentially treated with proteinase-K, magnetic beads and wash buffers. At the end of the process, the released RNA was dissolved in RNase free deionized water.

2.5.2. Inactivation of contaminating DNA

Any presence of residual DNA in a sample can give rise to false positive results. Therefore, an additional step of DNAase treatment was also performed to remove any DNA contamination. The DNA contamination was removed by incubating the extracted RNA with DNase-I enzyme. Each RNA sample was incubated at 37 °C for 10 min after adding 1 μl of DNase-I (Thermo Fisher Scientific, USA) followed by inactivation of DNase-1 at 75 °C for 10 min. A cDNA minus control was also included to exclude the possibility of

Table 1. PCR primer sequences, F (forward) R (reverse).

Sr. no	Gene	Primer sequence
1	Mur OPN-F	5′-TCTGATGAGACCGTCACTGC
2	Mur OPN-R	5′-AGGTCCTCATCTGTGGCATC
3	Mur-Col-1a1-F	5′-GAGAGGTGAACAAGGTCCCG
4	Mur-Col-1a1-R	5′-AAACCTCTCTCGCCTCTTGC
5	Mur GAPDH-F	5′-AAGGTCATCCCAGAGCTGAA
6	Mur GAPDH-R	5′-CTGCTTCACCACCTTCTTGA

non-specific amplification of contaminating DNA in the samples.

2.5.3. Synthesis of cDNA

MMLV reverse transcriptase (RT) (Thermo Fisher Scientific, USA) was the enzyme used for cDNA synthesis. The reaction conditions contained 2 μl RNA, 4 μl 5 X reaction buffer, 2 μl 10 mmol dNTPs mix (Thermo Fisher Scientific, USA), 1 μl primer (10 pmol μl^{-1}), 1 μl MMLV-RT (200 U μl^{-1}), 1 μl RNase inhibitor (20 U μl^{-1}), and 13 μl deionized water. Incubation was conducted at 42 °C for 30 min and RT inactivation at 70 °C for 5 min. Gene expression of Col type 1 and OPN was measured. The primer sequences of the genes are given in table 1 and primers were synthesized by Integrated DNA Technologies (IDT), USA.

2.5.4. RT-PCR analysis of osteoblastic markers

The PCR master mix was prepared in 0.2 ml PCR tubes. The volume of the reagents used to make up the PCR master mix and the reaction condition contents was as follows: 10 μl SYBER green PCR mix (Thermo Fisher, USA), 1 μl (10 pmol μl^{-1}) forward primer IDT (USA), 1 μl (10 pmol μl^{-1}) reverse primer (IDT, USA), 3 μl cDNA, and 5 μl DEPC treated water. Real-time PCR was conducted in a Rotor Gene-Q machine (Qiagen, USA) in a 20 μl reaction mix in 0.2 ml tubes. The samples were run with the following parameters: initial denaturation at 95 °C for 5 min and amplification of 35 cycles with denaturation at 95 °C for 15 s, annealing/extension at 60 °C for 50 s. GAPDH, a housekeeping gene, was run as the control. The Ct values of the target (OPN and Col) and the reference (GAPDH) genes were used for data analysis. The relative levels of mRNA expression were quantified by comparison with the internal control (GAPDH).

3. Results

3.1. Fourier transform infrared spectroscopy

The comparative FTIR spectra show (figures 1(a)–(d)) the characteristic peaks of HA. In nHA/E0, nHA/E30 and nHA/E50 spectra, the broad band in the range 3100–3400 cm^{-1} and the peak at 1640 cm^{-1} correspond to adsorbed water. The less intense peak of O–H was observed at 3570 cm^{-1}, whereas nHA-ht showed a stretching peak of O–H in the same region with high
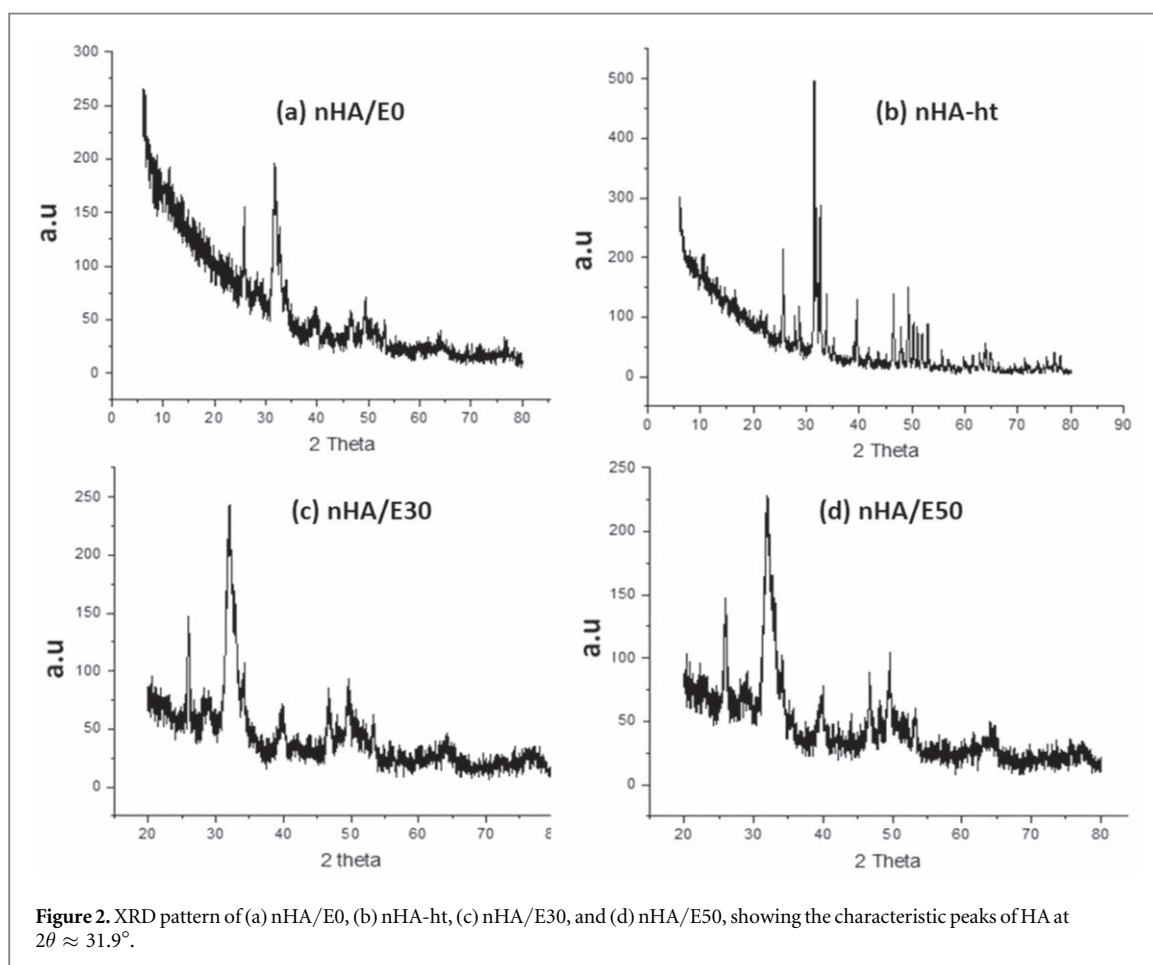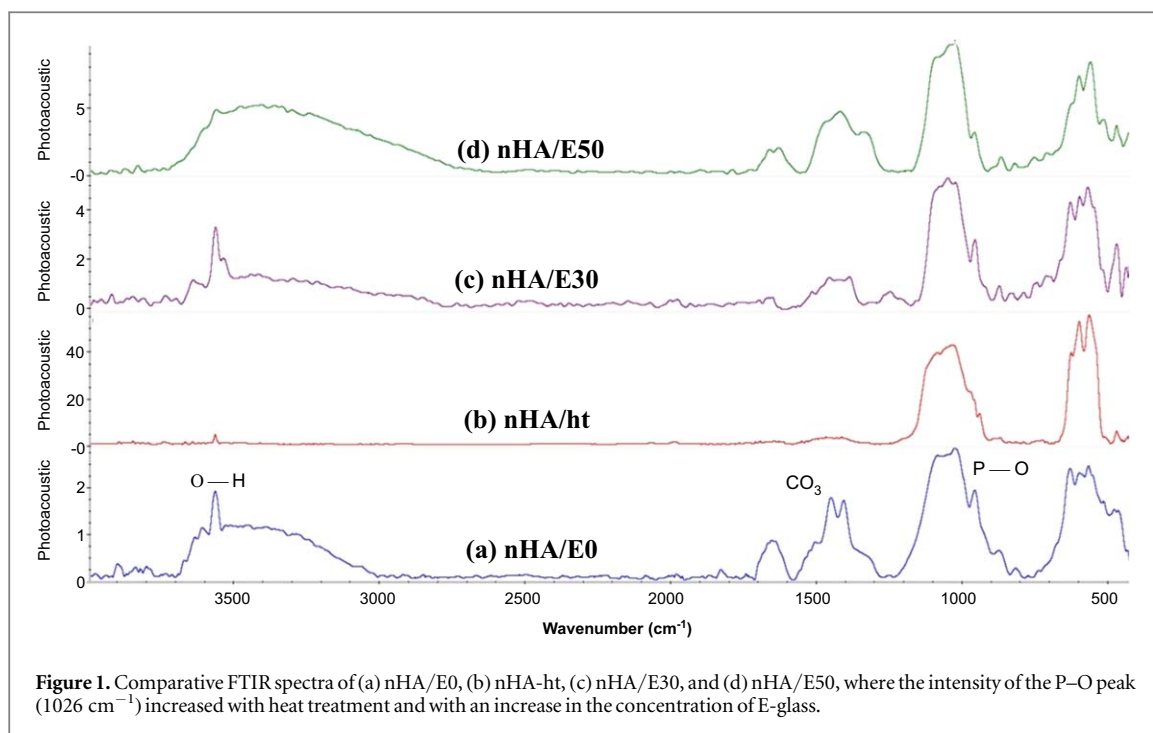
intensity. Peaks at 1455 cm^{-1} and 1412 cm^{-1} were attributed to adsorbed CO_3^{-2} ions on the surface and were observed in nHA/E0, nHA/E30, and nHA/E50; however, after heat treatment, the peaks became less intense. In addition, P–O was confirmed by characteristic peaks at 1095 cm^{-1}, 1053 cm^{-1}, 1026 cm^{-1}, 961 cm^{-1}, 564 cm^{-1} and 470 cm^{-1}. Peaks at 1095 cm^{-1} and 1026 cm^{-1} were assigned to the triply degenerated (v_3) asymmetric stretching mode of the P–O bond. The 961 cm^{-1} band indicated the non-degenerated (v_1) P–O symmetric stretching mode. A peak at 564 cm^{-1} revealed the presence of the triply degenerated (v_4) bending mode of the P–O–P bond. The intensity of the P–O peaks decreased with an increase in the concentration of E-glass fibers; however, no shifting of a peak was observed. The nHA-ht spectrum showed that peaks at 1095 cm^{-1} and 1040 cm^{-1} became substantially well defined, in accordance with the characteristic peaks of HA.

3.2. X-ray diffraction

The comparative XRD patterns of nHA/E0, nHA-ht, nHA/E30 and nHA/E50 are given in figures 2(a)–(d). The diffractogram of nHA-ht had a good match with the pattern for phase pure hydroxyapatite (JCPDS pattern 09-0432) and peak assignments were confirmed with the Miller index. The broad peaks in the XRD pattern of nHA/E0 at 25.96 (002) and 31.90 (211) indicated the amorphous nature of apatite. The change in the pattern of nHA up to 450 °C was not significant; however, when heat treated at 1000 °C, the peaks became intense and exhibited a crystalline structure. No phase impurity was observed in the nHA structure. The comparative nHA/E30 and nHA/E50 showed the characteristic peaks of HA and it was observed that the intensity of the peaks decreased with an increase in the concentration of E-glass. The intensity at the $2\theta \approx 31.90°$ peak of HA/E30 and HA/E50 was 245 and 225, respectively.

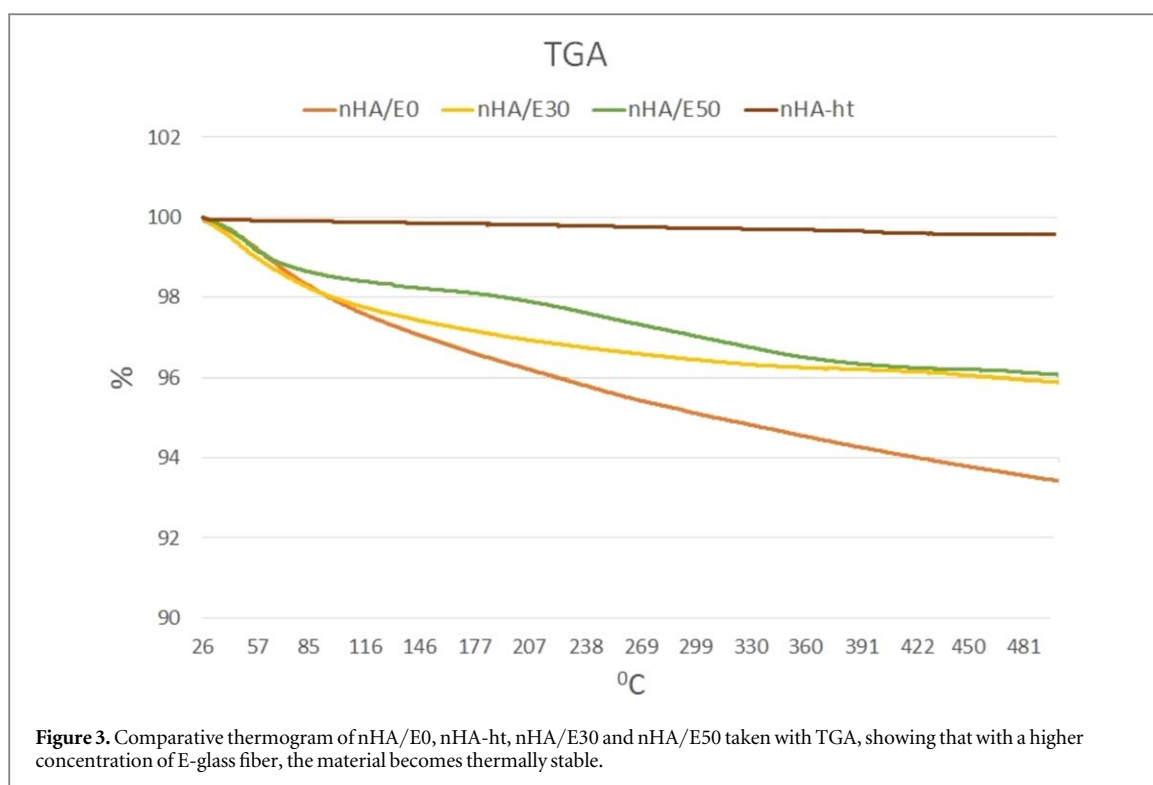### 3.3. Thermogravimetric analysis

The comparative weight loss profiles (TGA graphs) of nHA/E0, nHA-ht, nHA/E30, and nHA/E50 are shown in figure 3. The nHA/E0 showed a weight loss of almost 6.5% in this temperature range, whereas nHA-ht, nHA/E30 and nHA/E50 exhibited a weight loss of 0.5%, 5.1% and 4.9%, respectively. During the experimental reaction, ammonium nitrate (NH_4NO_3) was obtained as a by-product. The removal of NH_4NO_3 (M.P $\approx$ 170 °C) partly contributed to the weight loss up to 200 °C. The weight loss observed between 200 °C–280 °C was due to the removal of physically adsorbed water. At 300 °C, the nHA/E50 showed a weight loss of 3%, whereas nHA/E30 showed a loss of 4.5%, and hence the presence of a higher concentration of E-glass fiber made this material thermally stable.

Figure 1. Comparative FTIR spectra of (a) nHA/E0, (b) nHA-ht, (c) nHA/E30, and (d) nHA/E50, where the intensity of the P–O peak (1026 cm^{-1}) increased with heat treatment and with an increase in the concentration of E-glass.

Figure 2. XRD pattern of (a) nHA/E0, (b) nHA-ht, (c) nHA/E30, and (d) nHA/E50, showing the characteristic peaks of HA at $2\theta \approx 31.9°$.

3.4. Scanning electron microscopy

The SEM images of the E-glass fibers after heat treatment showed a smooth surface, as shown in figure 4(a). The samples were cut with a sharp blade and their edges maintained a smooth surface and the end surface showed an homogenous surface. The diameter of the E-glass fibers was 20 μm and the length was 250–500 μm. After nHA deposition on the E-glass fiber surface, it was observed that the surfaces were fully covered, as shown in figure 4(b). The size of the

Figure 3. Comparative thermogram of nHA/E0, nHA-ht, nHA/E30 and nHA/E50 taken with TGA, showing that with a higher concentration of E-glass fiber, the material becomes thermally stable.

deposited particle on both samples was approximately 50 nm and confirmed the deposition and attachment of nano-particles on the E-glass surface (figure 4(c)). The SEM image of nHA showed nano-structure particles and the observed size was 20–50 nm.

3.5. Cell viability

Figure 5 shows the cell growth (% variability) on all the tested samples. It was observed that after incubation, all samples showed a positive response; however, a non-significant difference ($p \geqslant 0.5$) was observed with periodic time intervals. For nHA samples, after three days, cell viability was 85.6% and after seven days, it was 90%. For nHA/E30, on day 3 and 7, cell viability was 98% and 100%, respectively, whereas for nHA/E50, it was 100% on both days. The % viability of nHA/E30 and nHA/E50 was significantly higher ($p \leqslant 0.05$) than nHA/E0. The SEM images (figures 6(A)—(C)) showed cell attachment and cells were spread on nHA/E0 and nHA/E-glass samples. It was observed that the cells adhered well to the surface of all the samples. Cell proliferation and morphology on the sample surfaces were observed after day 7 of culture, as shown in figures 6(D)–(F).

3.6. Osteogenesis analysis

The results of OPN and Col gene expression and the mathematical calculations of relative expression ratio (R) between the control (unexposed) and the test samples (exposed) are presented in tables 2 and 3, respectively. The highest OPN gene relative expression ratio was seen in nHA/E0 (15.4 ± 0.99) followed by nHA/E30 (7.56 ± 0.97) and nHA/E50 (4.57 ± 0.68).

The highest Col gene expression ratio was seen in nHA/E0 (15.9 ± 0.74) followed by nHA/E30 (4.53 ± 0.47) and nHA/E50 (2.75 ± 0.29). OPN and Col gene expression decreased significantly ($p < 0.001$) with a decreasing concentration of HA.

4. Discussion

Bioactive materials have been extensively used due to their structural support, cell delivery capability, and tissue regeneration possibilities. In this study, the surface grafting of E-glass fiber with nHA has been successfully achieved by using the microwave irradiation technique. FTIR and XRD confirmed the presence of nHA on the E-glass surface and, with an increase in the concentration of E-glass, changes were observed in the intensity of the peaks and crystallinity. The microwave conditions were optimized and set at 1000 W for 3 min because, at these conditions, microwaves are not able to change the molecular structure. Therefore, the resulting materials, i.e. nHA/E30 and nHAE50, were achieved in a short time with less chance of side reactions. In this study, surface activated E-glass was used and silica as the main component was abundantly present on the surface and it is anticipated that silica was covered with hydroxyl (OH) groups to form silanols (either free or bonded with neighboring silanol). The microwave irradiation technique was used purposely because, when E-glass was exposed to a microwave along with hydroxyapatite solution, di-electric heating of polar $-OH^-$ and silanol groups might result in energy transfer from these groups to the surrounding molecules. Therefore, while these
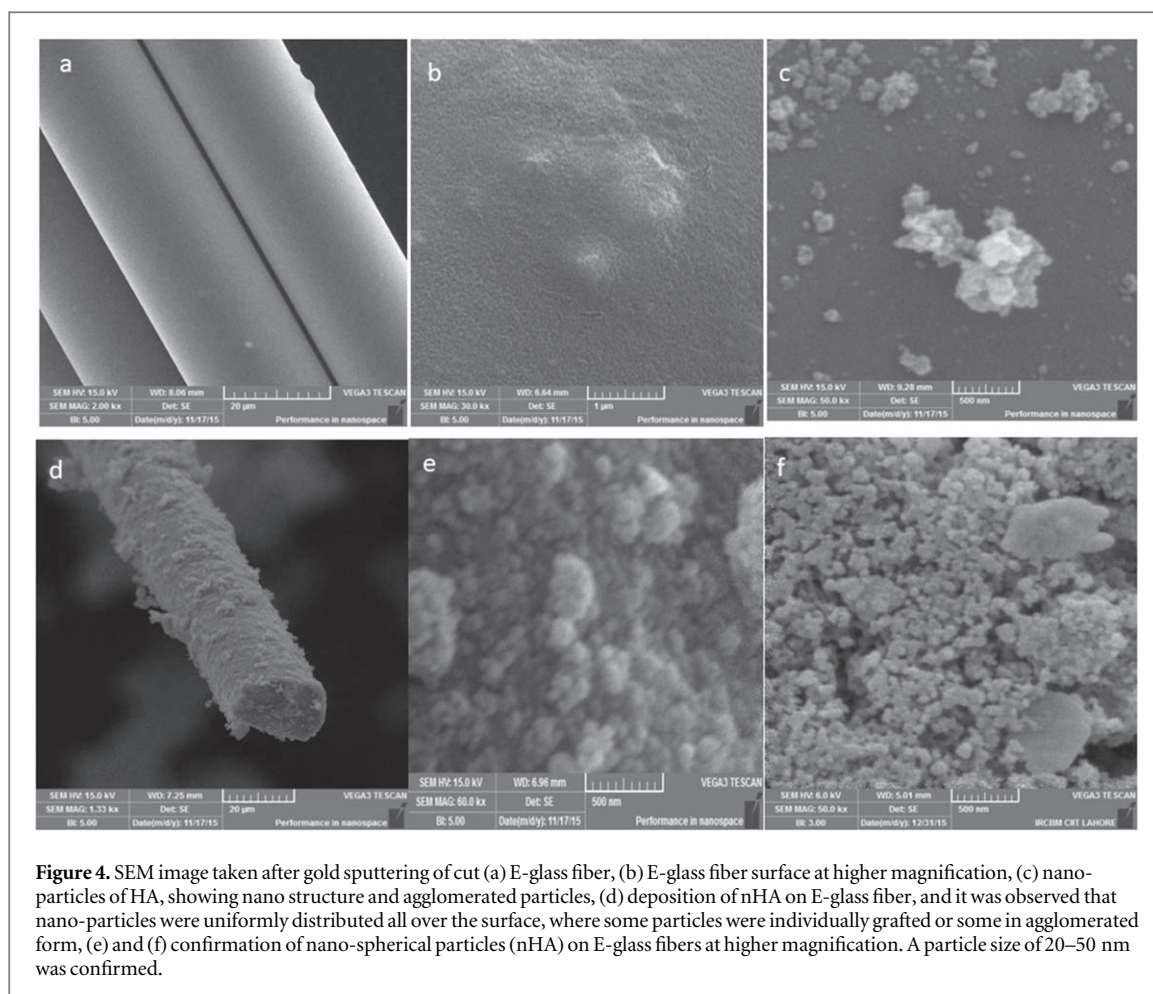
Figure 4. SEM image taken after gold sputtering of cut (a) E-glass fiber, (b) E-glass fiber surface at higher magnification, (c) nano-particles of HA, showing nano structure and agglomerated particles, (d) deposition of nHA on E-glass fiber, and it was observed that nano-particles were uniformly distributed all over the surface, where some particles were individually grafted or some in agglomerated form, (e) and (f) confirmation of nano-spherical particles (nHA) on E-glass fibers at higher magnification. A particle size of 20–50 nm was confirmed.

functional groups were microwave activated, it subsequently transferred energy to the groups present in the hydroxyapatite and stimulated the nHA adhesion on the E-glass surface. After synthesis of nHA/E glass, the resulting materials were heat treated at 450 °C to remove any unreacted ammonia and water molecules present on the surface. It is reported that the sub-surface water desorbed at 300 °C [23]. It is anticipated that the heat treatment of the E-glass-based material at high temperatures might change the physical and mechanical properties; however, the precise mechanism that contributes to the strength loss of heat-treated glass fiber is not yet fully established. It is reported that holding the fiber at around 500 °C causes a contraction and loss of strength [24, 25]. The increase in temperature is inversely proportional to the micro-porosity and affects the surface area, and subsequently, the bioactive properties of nHA. Heat treatment at 450 °C did not convert into a dense structure, therefore, it is expected that the nHA particles on the surface were porous and the porosity is necessary to stimulate the apatite deposition. SEM images showed a homogenous presence of nano spherical particles onto the cleanly cut E-glass fiber surface. Agglomerated particles were also observed and, due to a high surface energy of these nanoparticles, they tend to agglomerate to diminish this energy. The nanoscale-engineered surface can modulate and control the interactions between biomedical materials and biological tissues. Further, nHA promotes ion exchange with the physiological environment and improves cellular response [26]. The nanoparticles have a high surface area and it promotes chemical interaction with the organic matrix. Thus, the binding capacity of these experimental bioactive E-glass fibers and matrix would be enhanced during fabrication of the composites for restoration and implant applications. The incorporation of these bioactive fibers will not only enhance the mechanical properties but also play a significant role in achieving a biomimetic approach.

The prepared nHA/E-glass materials showed compatibility with cells and the presence of E-glass enhanced cell viability. The cells were proliferated on the surface, as shown in the SEM images, and a multi-layered cell matrix could be observed at day 7. Culturing cells directly on the surface of nHA/E-glass indicated the synergistic interaction of cells with nHA and E-glass fibers. The nHA is considered to be a hydrophilic material and this property, along with porosity and roughness, affect the cell behavior [27]. The adhered morphological cells spread with some extensions indicating better attachment of cells on the material surface. The surfaces of the pellets showed the development of a new layer as the samples were
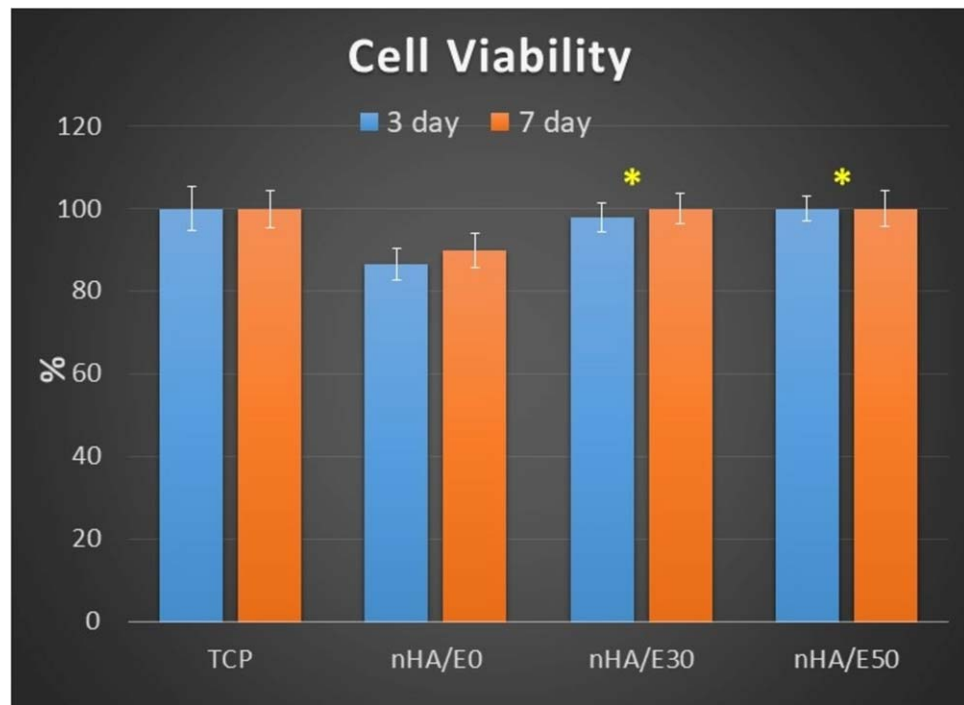
Figure 5. Cell viability (%) of nHA/E0, nHA/E30, and nHA/E50 at day 3 and 7, where nHA/30 and nHA/50 showed significantly higher $^*(p \leqslant 0.5)$ % viability compared to nHA; however, a non-significant difference was observed with periodic time intervals.
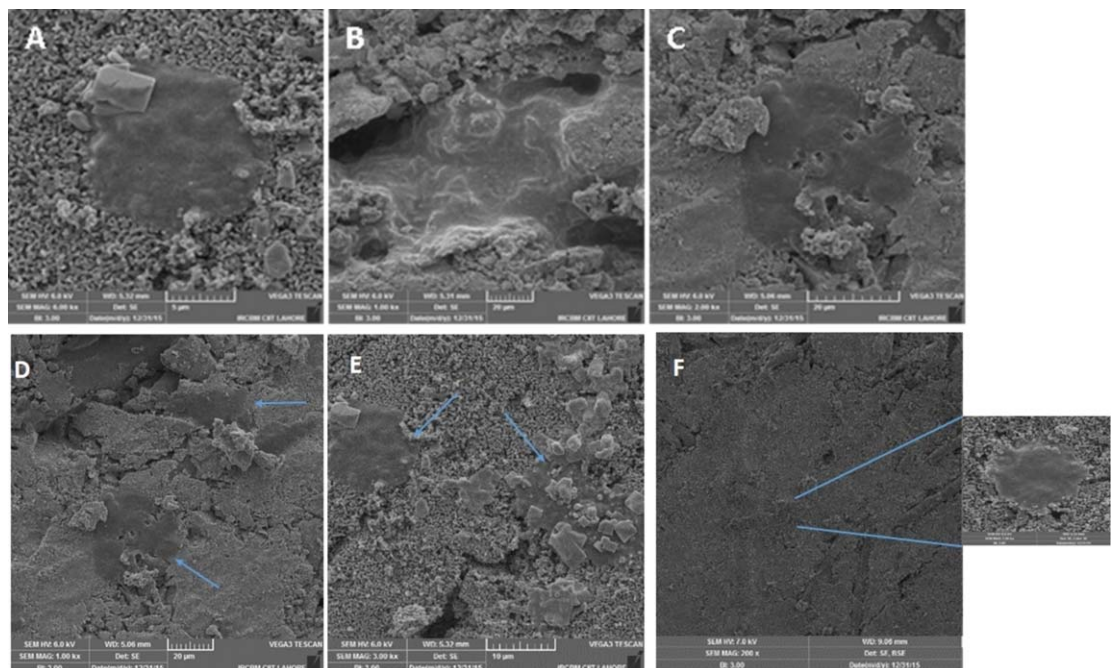

Figure 6. SEM images of cell attachment on samples discs. The samples were fixed formalin and the images were taken at different magnification. The images of samples (A) nHA/E0, (B) nHA/E30, (C) nHA/E50 and (D)–(F) showing proliferation and adherence of cells on surface.

immersed in culture media. The cell culturing media in a static condition has a tendency to favor the dissolution process of nHA [28], and afterwards, the precipitation of ions due to mineral nucleation theory and it promotes a formation of a new apatite layer over the surface.

This study dealt with a novel combination of nHA and E-glass fibers and its ability for use as a scaffold for tissue engineering and clinical applications. MC3T3-E1 cells were used as they are osteoblastic in nature and capable of forming mineralized bone tissue *in vitro* [29]. The results of this study clearly indicate that nHA/E0 and

Table 2. Summary of the results of Ct and ratio (R) of OPN gene expression in murine osteoblasts exposed to various concentrations of E-glass and nano-hydroxyapatite (nHA).

E-Glass	HA	Gene	Ct test	Ct control	ΔCt[a]	$2.0^{\Delta Ct}$	Ratio (R)[b]	Expression%
nHA/E0	100%	Target (OPN)	27.15	16.81	−10.34	0.000 77	15.4 ± 0.99	100%
		Reference (GAPDH)	31.41	17.23	−14.18	0.000 05		
nHA/E30	70%	Target (OPN)	24.36	16.81	−7.55	0.005 35	7.56 ± 0.97	51.9%
		Reference (GAPDH)	27.68	17.23	−10.45	0.000 72		
nHA/E50	50%	Target (OPN)	21.66	16.81	−4.85	0.034 72	4.57 ± 0.68	29.4%
		Reference (GAPDH)	24.26	17.23	−7.03	0.007 65		

a (Ct control—Ct test)
b $2.0^{\Delta Ct \text{ (target)}}/2.0^{\Delta Ct \text{ (reference)}}$

Table 3. Summary of the results of Ct and ratio (R) of Col gene expression in murine osteoblast exposed to various concentrations of E-glass and nano-hydroxyapatite (nHA).

E-Glass	HA	Gene	Ct test	Ct control	ΔCt[a]	$2.0^{\Delta Ct}$	Ratio (R)[b]	Expression %
nHA/E0	100%	Target (Col)	27.16	19.92	−7.24	0.006 62	15.93 ± 0.74	100%
		Reference (GAPDH)	31.40	20.18	−11.22	0.000 42		
nHA/E30	70%	Target (Col)	30.19	19.92	−10.27	0.000 80	4.53 ± 0.47	28.03%
		Reference (GAPDH)	32.59	20.18	−12.41	0.000 18		
nHA/E50	50%	Target (Col)	28.51	19.92	−8.58	0.002 61	2.75 ± 0.29	17.63%
		Reference (GAPDH)	30.22	20.18	−10.04	0.000 94		

a (Ct control—Ct test)
b $2.0^{\Delta Ct \text{ (target)}}/2.0^{\Delta Ct \text{ (reference)}}$

novel nHA/E-glass fibers were highly osteogenic in nature and supported the growth of murine osteoblasts. The PCR results were expressed as a ratio of gene expression between the murine osteoblasts exposed and unexposed to the osteogenic material. The relative quantification method was used and a normally expressed 'housekeeping' gene (GAPDH) was used. In order to understand the physiological changes in gene expression, it is recommended that relative quantification is performed. OPN is a 34 kDa highly phosphorylated glycoprotein which forms a major component of bone, and it progressively develops during the formation and remodeling of bone [30]. The highest relative expression ratio of OPN by MC3T3 E-1 cells was seen for nHA/E0. This could be attributed to the osteogenic nature of nHA, which allowed the attachment, proliferation, and differentiation of the murine osteoblasts.

The relative expression ratio for OPN decreased as the concentration of E-glass fibers increased. There was a significant difference among the ratios in nHA/E0, nHA/E30, and nHA/E50. This showed that the nHA/E50 stimulated the cells only 4.57-fold compared to the control. As the concentration of E-glass fibers in the discs increased, likewise the concentration of nHA was reduced. This reduced the osteogenic content as E-glass fibers are inherently inert [3]; however, these fibers supported the growth of cells and did not restrict their proliferation.

The results for Col gene expression in all the materials followed a similar pattern to OPN. The highest ratio was seen in nHA/E0 followed by nHA/E30 and nHA/E50. This trend further augments the ability of the novel material to induce osteoblastic cells to express Col. The expression of Col further proved that the cells were

proliferating and were also able to maintain their phenotype. nHA is osteoconductive and osteointegrative and, in some cases, osteoinductive [31]. It had effectively up-regulated the expression of both OPN and Col in this experiment and it is established that in the presence of nHA/E-glass the expression was observed. Only for nHA/E0, Col expression was slightly more as compared to OPN, whereas for both nHA/E30 and nHA/E50, OPN expression was greater in comparison to Col. When multiple genes are being expressed, they may have a competitive effect on each other and may not have an improved expression in all cases [32].

The gene expression profile of all samples was almost the same as all stimulated MC3T3 E-1 cells to proliferate and produce OPN and Col type 1. The adhesion of nHA on E-glass fibers has effectively imparted osteogenecity, which was the purpose of this novel biomaterial. It is expected that the higher concentration is enough to improve the mechanical properties without compromising the osteogenity of nHA. These results showed potential applications as an implant and reinforcing agent in restorative materials. Dental restorations and prosthesis are subjected to thousands of cycles of stress per day, therefore a new material with high mechanical (as expected) and bioactive properties is required which can tolerate the stress with a high reinforcing efficiency.

5. Conclusion

Spherical nanoparticles of HA were successfully deposited/adhered on E-glass fibers, and nHA/E-glass fibers were synthesized via the microwave irradiation method in the shortest time period. The presence of

E-glass fiber made nHA thermally stable; however, it is critical to know the temperature limit while preparing these materials. The cell viability test confirmed these materials to be biocompatible. It was concluded, on the basis of these results, that the novel material was osteogenic in nature and supported the growth of cells, OPN and Col, as measured by PCR. This concentration is enough to improve the other properties of nHA without compromising the osteogenity of nHA. It can be used as a scaffold for bone tissue engineering and/or after silanization (pilot study conducted) and it can be used as an implant and reinforcing agent in dental restorative materials.

Acknowledgments

ORCID iDs

Abdul Samad Khan ⓘ https://orcid.org/0000-0002-2165-800X

References

[1] Sönmez M, Georgescu M, Vâlsan M, Radulescu M, Ficai D, Voicu G, Ficai A and Alexandrescu L 2015 Design and characterization of polypropylene matrix/glass fibers composite materials *J. Appl. Polym. Sci.* **132** 42163

[2] Vallittu P K, Närhi T O and Hupa L 2015 Fiber glass–bioactive glass composite for bone replacing and bone anchoring implants *Dental Mater.* **31** 371–81

[3] Khan A S, Azam M T, Khan M, Mian S A and Ur Rehman I 2015 An update on glass fiber dental restorative composites: a systematic review *Mater. Sci. Eng.* C **47** 26–39

[4] Zhang M and Matinlinna J P 2012 E-glass fiber reinforced composites in dental applications *Silicon* **4** 73–8

[5] Vakiparta M, Puska M and Vallittu P K 2006 Residual monomers and degree of conversion of partially bioresorbable fiber-reinforced composite *Acta Biomaterialia* **2** 29–37

[6] Moritz N, Strandberg N, Zhao D S, Mattila R, Paracchini L, Vallittu P K and Aro H T 2014 Mechanical properties and *in vivo* performance of load-bearing fiber-reinforced composite intramedullary nails with improved torsional strength *J. Mech. Behav. Biomed. Mater.* **40** 127–39

[7] Vallittu P and Lassila V 1992 Reinforcement of acrylic resin denture base material with metal or fibre strengtheners *J. Oral Rehabil.* **19** 225–30

[8] Ballo A M, Akca E A, Ozen T, Lassila L, Vallittu P K and Narhi T O 2009 Bone tissue responses to glass fiber-reinforced composite implants—a histomorphometric study *Clin. Oral Implants Res.* **20** 608–15

[9] Abdulmajeed A A, Lassila L V, Vallittu P K and Närhi T O 2011 The effect of exposed glass fibers and particles of bioactive glass on the surface wettability of composite implants *Int. J. Biomater.* **2011** 607971

[10] Tuusa S M, Peltola M J, Tirri T, Lassila L V and Vallittu P K 2007 Frontal bone defect repair with experimental glass-fiber-reinforced composite with bioactive glass granule coating *J. Biomed. Mater. Res.* B **82** 149–55

[11] Vallittu P K, Narhi T O and Hupa L 2015 Fiber glass-bioactive glass composite for bone replacing and bone anchoring implants *Dental Mater.* **31** 371–81

[12] Gibson I R 2015 *Hydroxyapatite (Hap) for Biomedical Applications* (New York: Elsevier) pp 269–87

[13] Enax J and Epple M 2018 Synthetic hydroxyapatite as a biomimetic oral care agent *Oral Health Prev. Dent.* **16** 7–19

[14] Santos M H, Oliveira M d, Souza L P d F, Mansur H S and Vasconcelos W L 2004 Synthesis control and characterization of hydroxyapatite prepared by wet precipitation process *Mater. Res.* **7** 625–30

[15] Monmaturapoj N 2017 Nano-size hydroxyapatite powders preparation by wet-chemical precipitation route *J. Metals Mater. Miner.* **18** 15–20

[16] Khan A, Ahmed Z, Edirisinghe M, Wong F and Rehman I 2008 Preparation and characterization of a novel bioactive restorative composite based on covalently coupled polyurethane–nanohydroxyapatite fibres *Acta Biomaterialia* **4** 1275–87

[17] Nazir R, Khan A S, Ahmed A, Ur-Rehman A, Chaudhry A A, Rehman I U and Wong F S 2013 Synthesis and *in-vitro* cytotoxicity analysis of microwave irradiated nano-apatites *Ceram. Int.* **39** 4339–47

[18] Khan A, Wong F, McKay I, Whiley R and Rehman I 2013 Structural, mechanical, and biocompatibility analyses of a novel dental restorative nanocomposite *J. Appl. Polym. Sci.* **127** 439–47

[19] Smith D C, Pilliar R M and Chernecky R 1991 Dental implant materials. I. Some effects of preparative procedures on surface topography *J. Biomed. Mater. Res.* **25** 1045–68

[20] Das S, Mukhopadhyay A, Datta S and Basu D 2009 Prospects of microwave processing: an overview *Bull. Mater. Sci.* **32** 1–13

[21] Khan A, Hussain A, Sidra L, Sarfraz Z, Khalid H, Khan M, Manzoor F, Shahzadi L, Yar M and Rehman I 2017 Fabrication and *in vivo* evaluation of hydroxyapatite/carbon nanotube electrospun fibers for biomedical/dental application *Mater. Sci. Eng.* C **80** 387–96

[22] Lung C Y, Sarfraz Z, Habib A, Khan A S and Matinlinna J P 2016 Effect of silanization of hydroxyapatite fillers on physical and mechanical properties of a bis-GMA based resin composite *J. Mech. Behav. Biomed. Mater.* **54** 283–94

[23] Nishioka G M and Schramke J A 1985 Thermodesorption of water from silicate surfaces *J. Colloid Interface Sci.* **105** 102–11

[24] Thomason J L, Kao C C, Ure J and Yang L 2014 The strength of glass fibre reinforcement after exposure to elevated composite processing temperatures *J. Mater. Sci.* **49** 153–62

[25] Thomason J, Jenkins P and Yang L 2016 Glass fibre strength—a review with relation to composite recycling *Fibers* **4** 18

[26] Barros J, Grenho L, Manuel C M, Ferreira C, Melo L, Nunes O C, Monteiro F J and Ferraz M P 2014 Influence of nanohydroxyapatite surface properties on Staphylococcus epidermidis biofilm formation *J. Biomater. Appl.* **28** 1325–35

[27] Chan Y H, Lew W Z, Lu E, Loretz T, Lu L, Lin C T and Feng S W 2018 An evaluation of the biocompatibility and osseointegration of novel glass fiber reinforced composite implants: *in vitro* and *in vivo* studies *Dental Mater.* **34** 470–85

[28] da Silva H M, Mateescu M, Ponche A, Damia C, Champion E, Soares G and Anselme K 2010 Surface transformation of silicon-doped hydroxyapatite immersed in culture medium under dynamic and static conditions *Colloids Surf.* B **75** 349–55

[29] Czekanska E M, Stoddart M J, Ralphs J R, Richards R and Hayes J 2014 A phenotypic comparison of osteoblast cell lines versus human primary osteoblasts for biomaterials testing *J. Biomed. Mater. Res.* A **102** 2636–43

[30] Chen J, Singh K, Mukherjee B B and Sodek J 1993 Developmental expression of osteopontin (OPN) mRNA in rat tissues: evidence for a role for OPN in bone formation and resorption *Matrix* **13** 113–23

[31] Gerhardt L-C and Boccaccini A R 2010 Bioactive glass and glass-ceramic scaffolds for bone tissue engineering *Materials* **3** 3867–910

[32] Xu M, Zhang Y, Zhai D, Chang J and Wu C 2013 Mussel-inspired bioactive ceramics with improved bioactivity, cell proliferation, differentiation and bone-related gene expression of MC3T3 cells *Biomater. Sci.* **1** 933–41